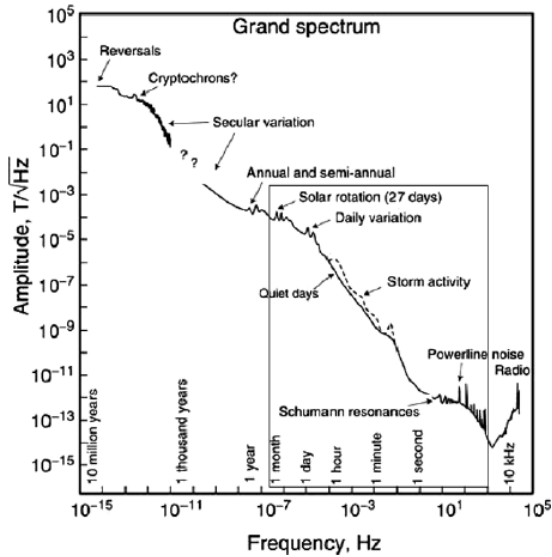


ULF waves as a possible stray field source for CLIC

Balázs Heilig
Mining and Geological Survey of Hungary
MBFSz

ULF waves



~~The Entire Electromagnetic Radio Spectrum~~

ELF	SLF	ULF	VLF	LF	MF	HF	VHF	UHF	SHF	EHF
3 Hz	30 Hz	300 Hz	3 kHz	30 kHz	300 kHz	3 MHz	30 MHz	300 MHz	3 GHz	30 GHz
30 Hz	300 Hz	3 kHz	30 kHz	300 kHz	3 MHz	30 MHz	300 MHz	3 GHz	30 GHz	300 GHz

ELF-VLF phenomena
J. Lichtenberger

ULF waves in space physics

~ 1 mHz to few Hz

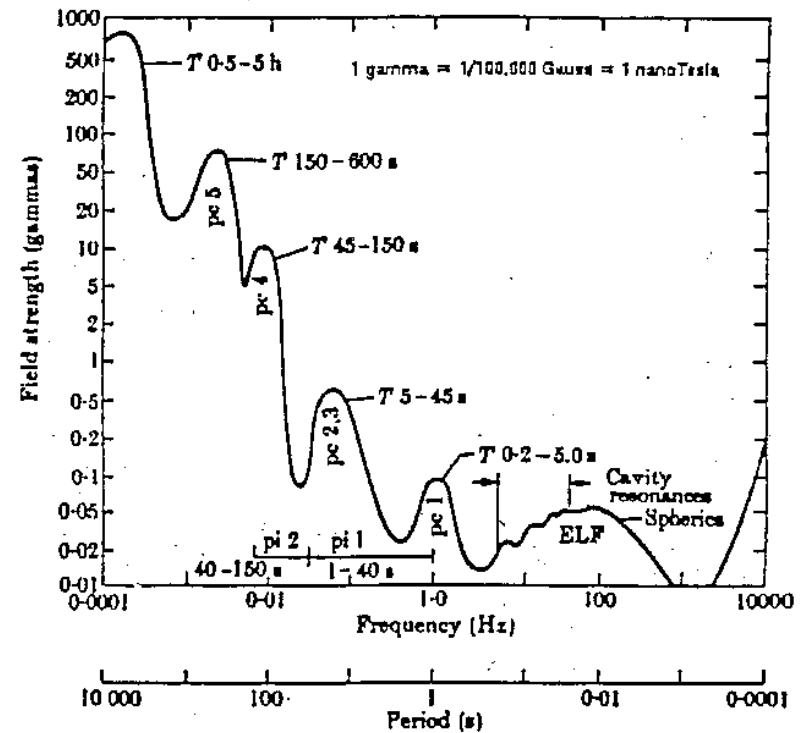
first observed in 1859 [great aurora](#) events
(Stewart, 1861)

ULF waves (geomagnetic pulsations)

- Classification (morphology)

(c=continuous, i=irregular) and period of the pulsation (Jacobs et al., 1964):

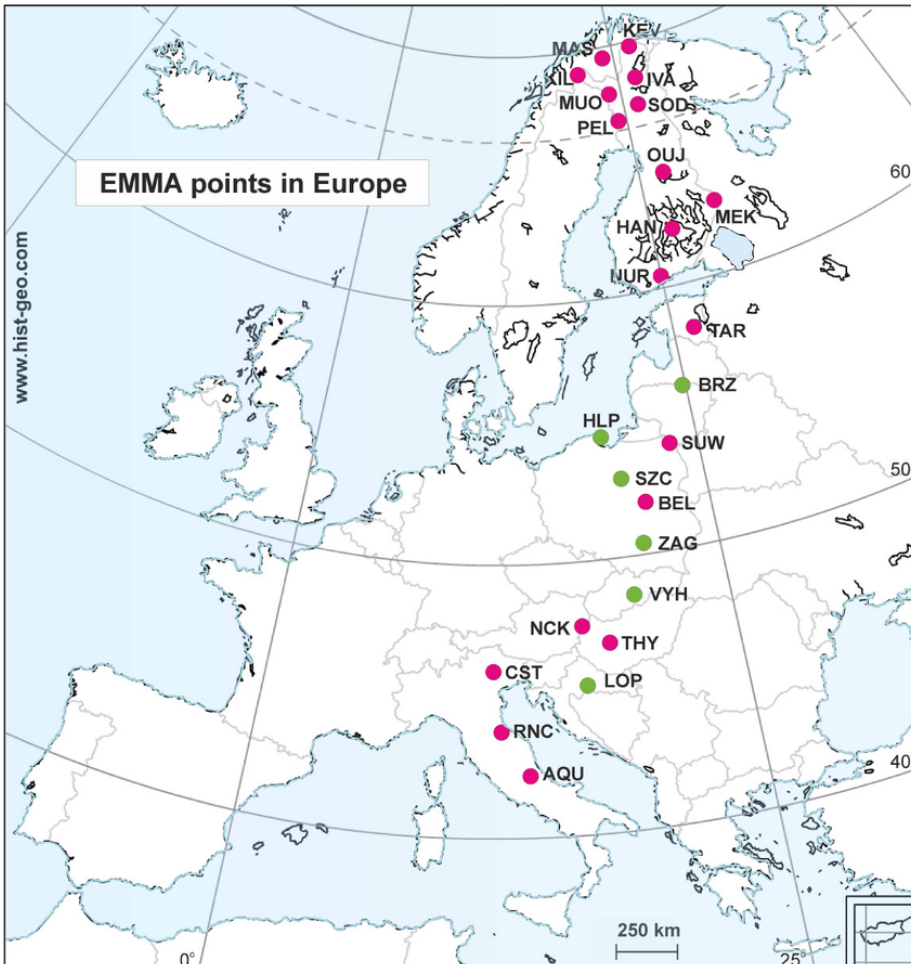
MAGNITUDE OF THE GEOMAGNETIC PULSATIONS IN RANGE 0.0001 - 10 kHz



	Pc 1	Pc 2	Pc 3	Pc 4	Pc 5	Pi 1	Pi 2
T [s]	0.2-5	5-10	10-45	45-150	150-600	1-40	40-150
f	0.2-5 Hz	0.1-0.2 Hz	22-100 mHz	7-22 mHz	2-7 mHz	0.025-1 Hz	2-25 mHz

Ground observations of ULF waves

EMMA <http://geofizika.canet.hu/plasmon/emmaplot.php>

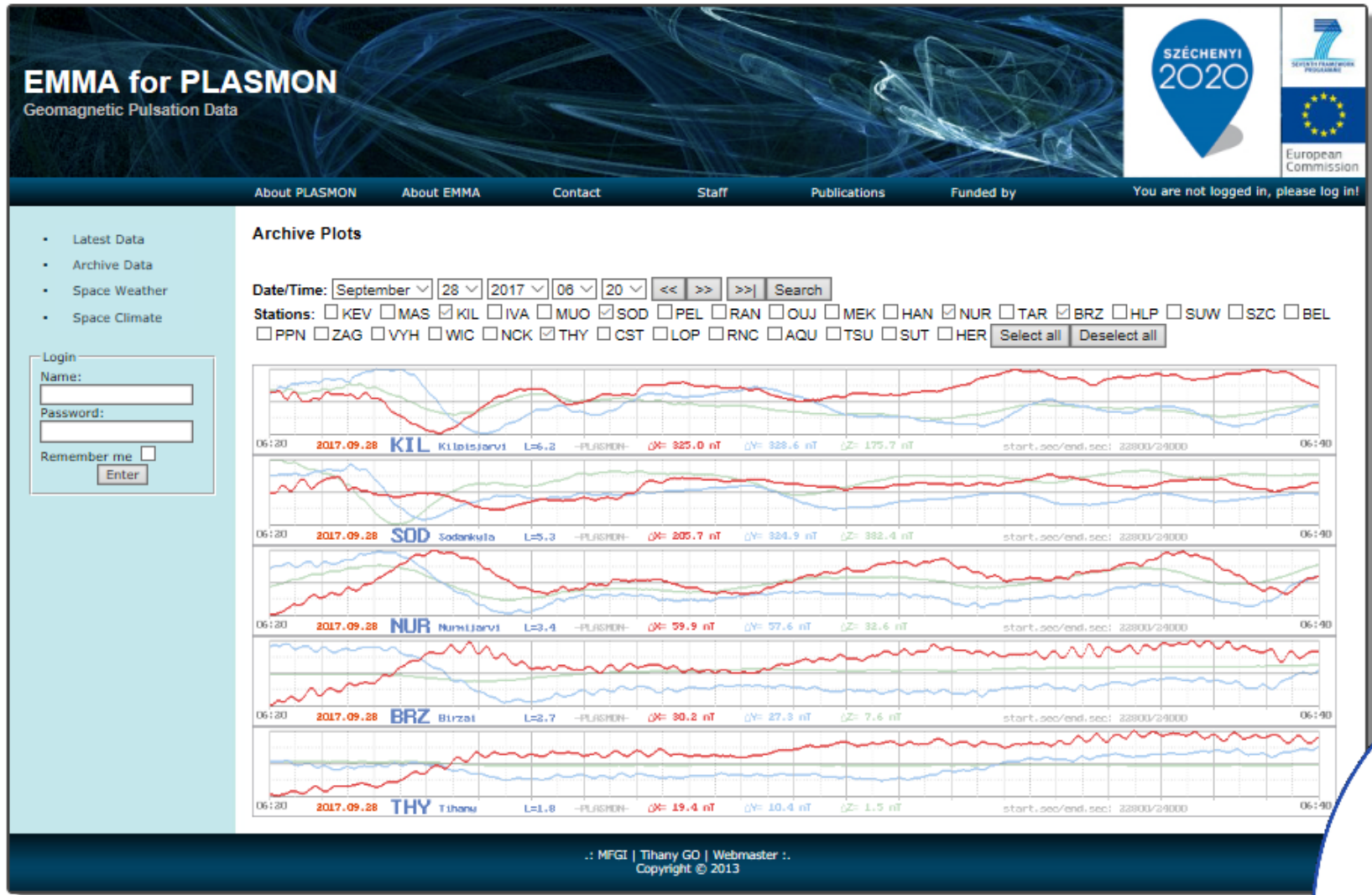


EMMA is a meridional magnetometer array for ULF studies established in 2011

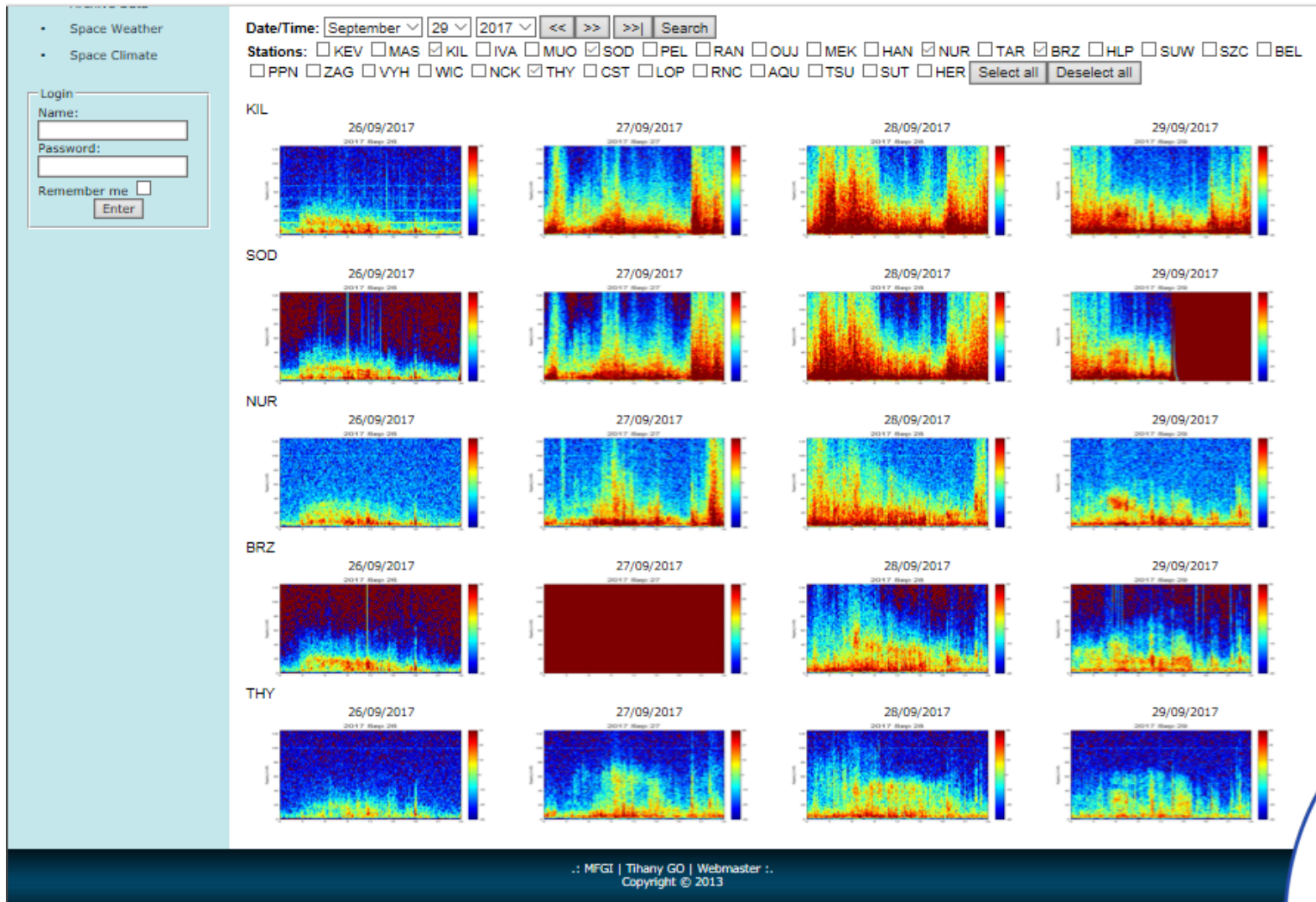
ULF waves as observed on the ground are latitude dependent (as many of the space weather phenomena)

Ground observations of ULF waves

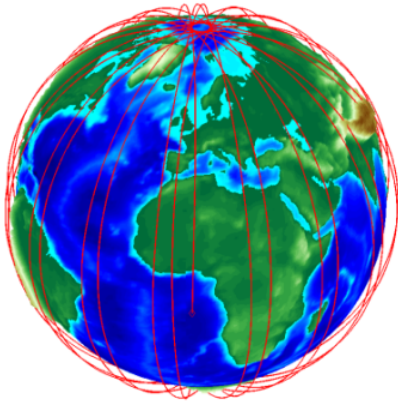
latitude dependent amplitudes/frequencies



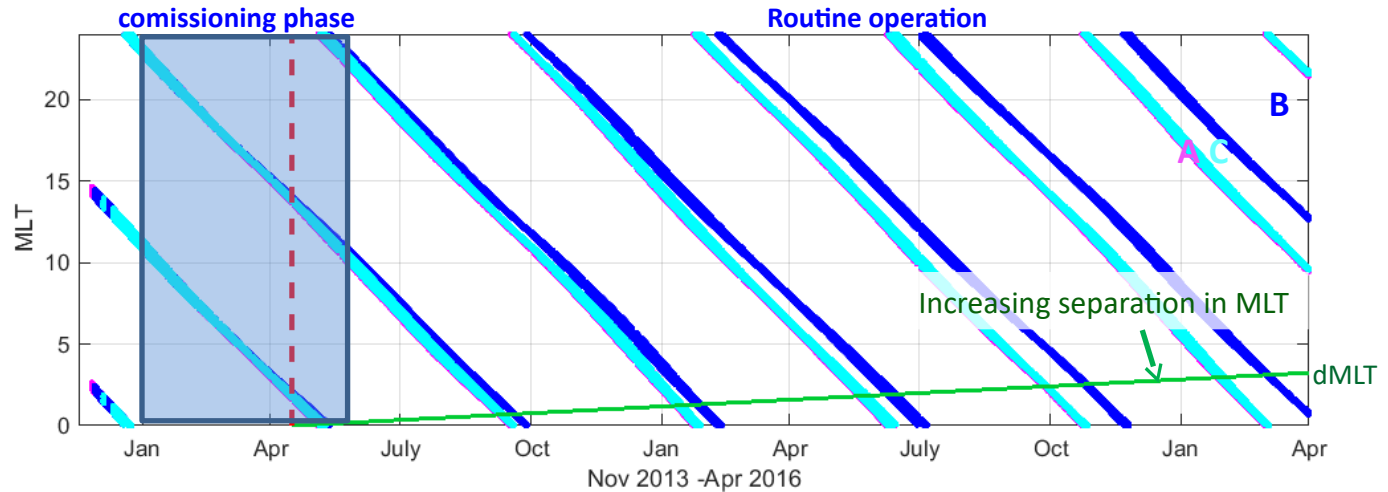
Ground observations of ULF waves



Space observations of ULF waves



Daily orbit of a Swarm sc



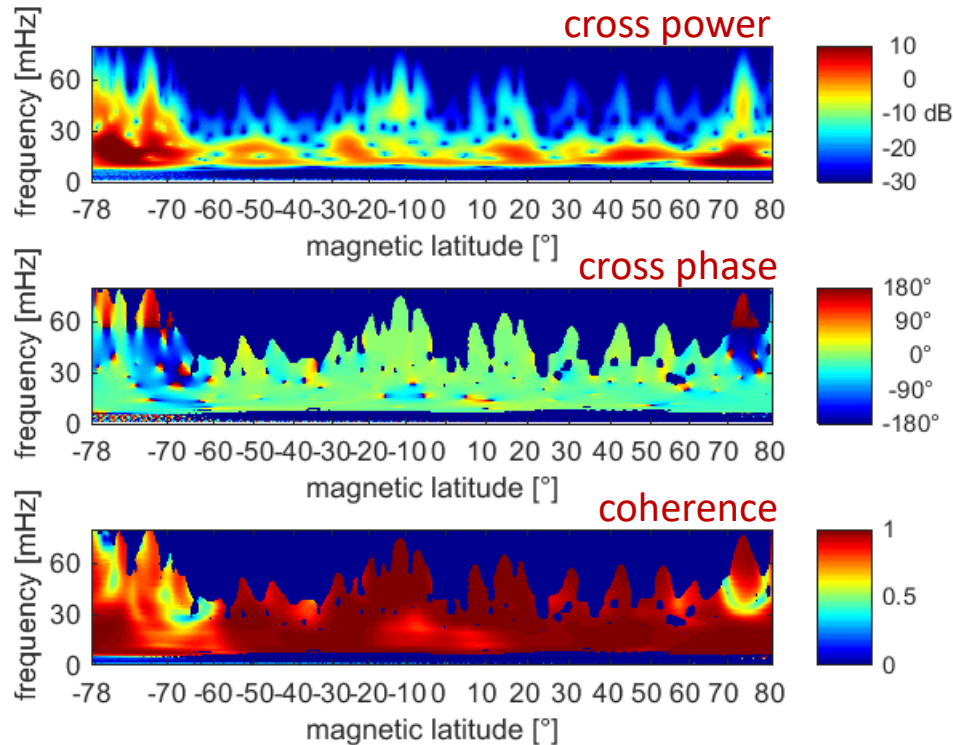
Slow MLT drift of Swarm A, B and C

- * launch: on 22 Nov 2013
- * orbital period: ~ 95 min ($\sim 4^\circ$ latitude/1 min)
- * routine operation (from mid April 2014)
 - A and C side by side (1° - 1.5° EW separation) at $480 \rightarrow 455$ km altitude, inclination: 87.4°
 - B at $525 \rightarrow 515$ km altitude, inclination: 87.8°
- * Increasing separation in MLT



Swarm trio

Wavelet coherence and cross phase (dayside pole-to-pole example)



A-C wavelet cross power, phase difference, coherence
19 April 2014 01:03-01:42

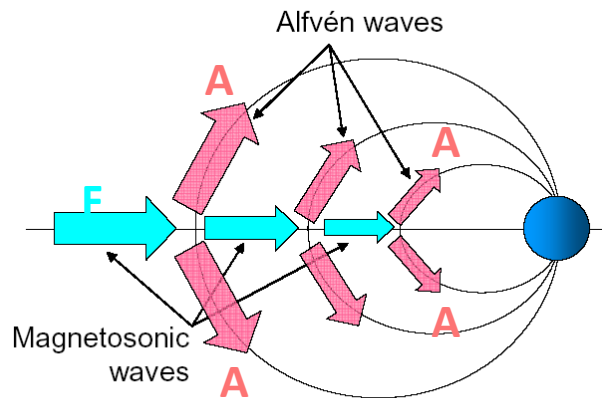
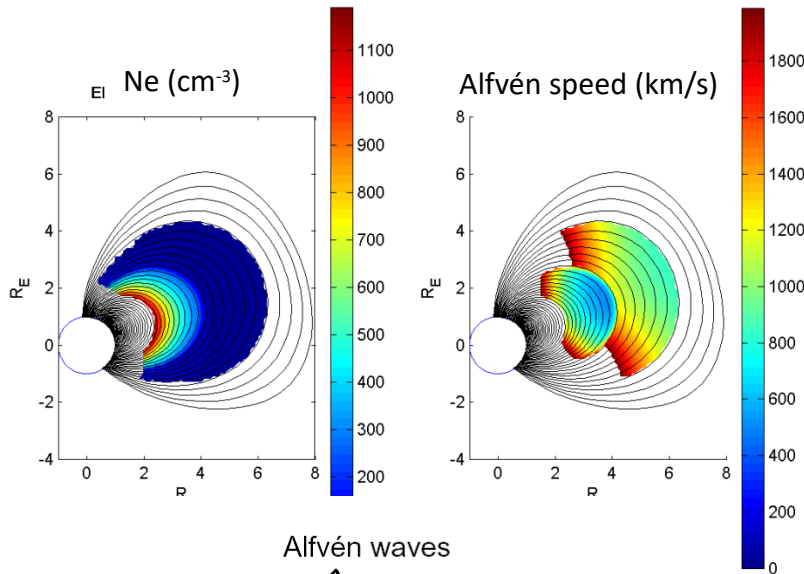
Latitudinal separation: $0.5-0.6^\circ$ ($dt = 8-10$ s)

Phase shift: 180° at 55 mHz ($T = 18$ s) $\rightarrow dt = 9$ s \rightarrow spatial structure



Swarm trio

Simple model: linear MHD in cold plasma



(Ponomarenko et al. 2005, AnnGeo)

Two wave modes exist in cold plasma MHD

F Compressional / magnetosonic / fast mode
 propagates isotropically
 it has a longitudinal component
 pressure fluctuations

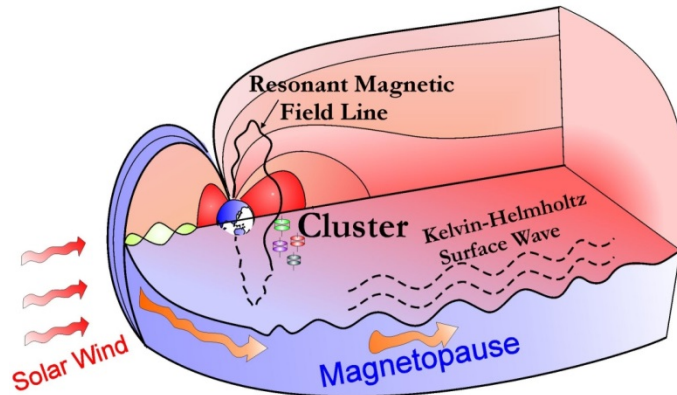
(shear) Alfvén mode
 propagates along field lines
 transverse (to the field line)
 components
 carries a field aligned current

Characteristic speed: **Alfvén speed**

$$v_A = \frac{B}{\sqrt{\mu_0 \rho}}$$

B – magnetic field strength , ρ - plasma mass density

Sources of ULF waves: 1. external (examples)



Kelvin-Helmholtz waves (solar wind shear)

Kelvin-Helmholtz instability

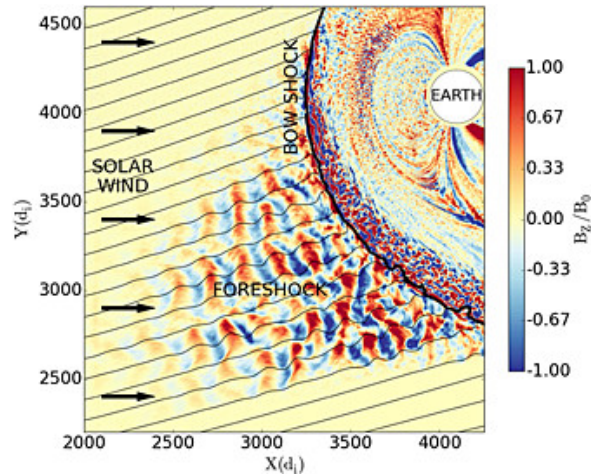
Surface wave

exponential decay in the magnetosphere
can reach only on outer shells (in space) /

high latitude (on ground)

morning and evening maxima

Pc4-Pc5



Ion-cyclotron resonance

Compressional mode in the magnetosphere

propagation isotropic with Alfvén speed

prenoon maximum

ion cyclotron origin $\rightarrow f \sim |B_{imf}|$

(interplanetary magnetic field, B_{imf})

Pc3-(Pc4)

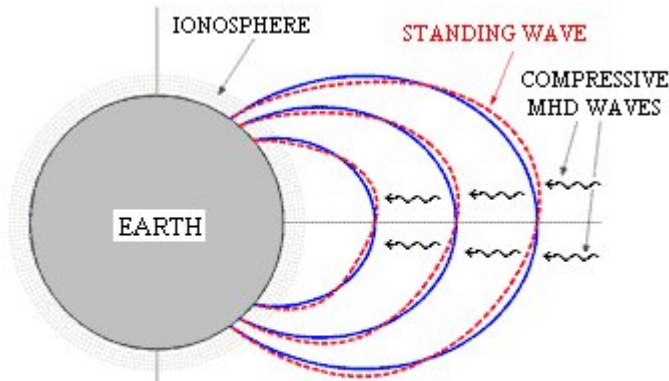
power: solar wind speed, density,

orientation of B_{imf}

(Heilig, Lühr, Rother, 2007, Annales Geophysicae)

Upstream waves driven by ion-cyclotron resonance (Doppler shifted, average $M_A \sim 8$)

Sources of ULF waves: 2. internal (examples)



Compressional waves **couple** to standing Alfvén waves if its frequency matches the eigenfrequency of the field line

The **wavelength** of ULF waves is **comparable** to the **size of the magnetosphere** (length of field lines)

Resonances

- standing waves along field lines (**field line resonances**): Pc3-Pc5
- **cavity mode resonances (Pc3-4)**
- waveguide modes

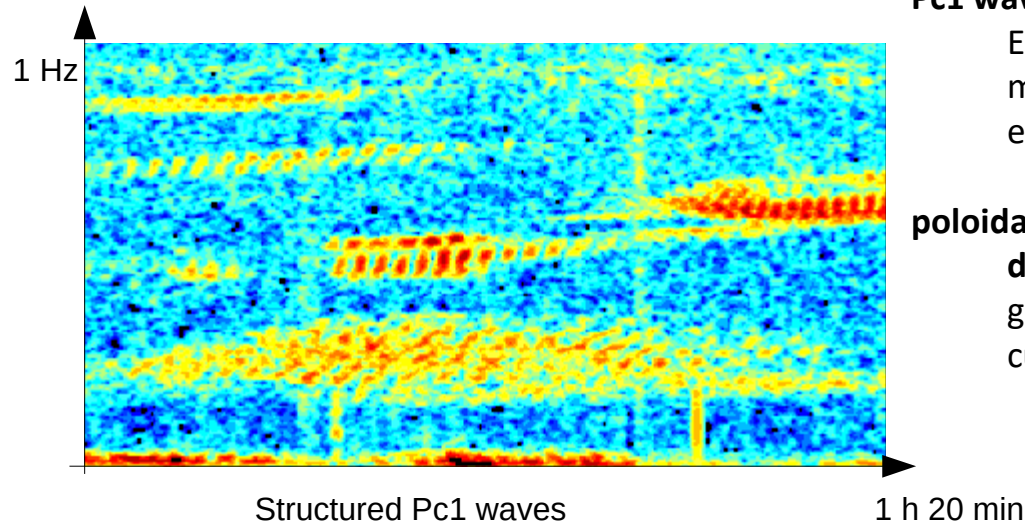
Waves driven by kinetic effects, instabilities

Pc1 waves (few Hz)

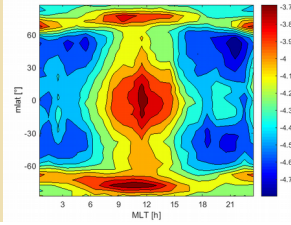
- EMIC waves (ion-cyclotron waves in the magnetosphere)
- energetic protons ring current (10-100 keV)

poloidal Pc5 (high-m)

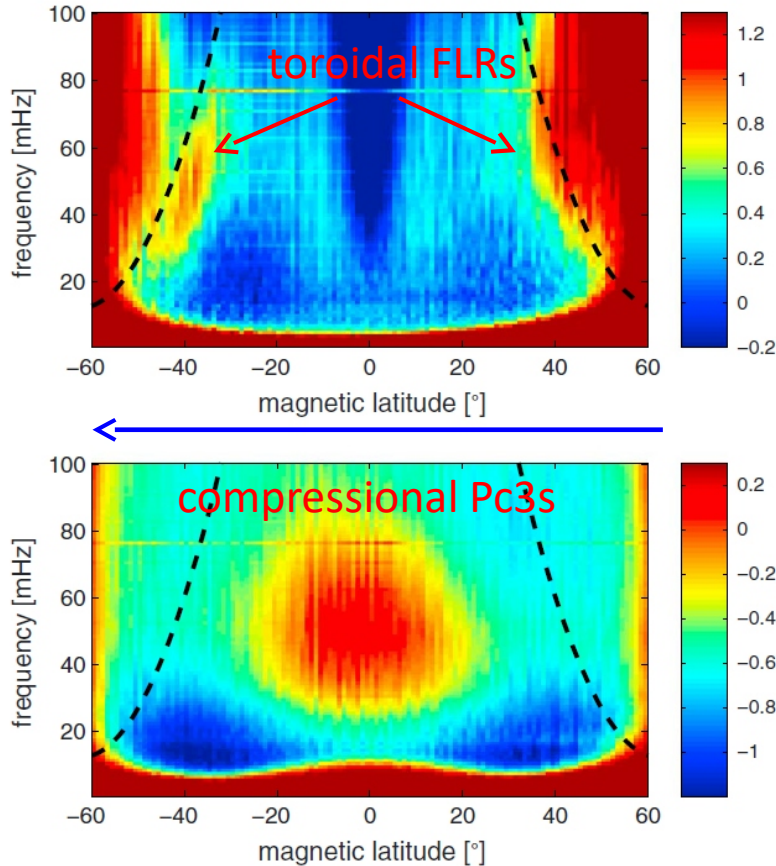
- drift-bounce resonance** due to pressure gradient, magnetic field gradient and curvature



Pc3 (20-100 mHz) waves in the topside ionosphere redistribution of incoming wave energy through resonant absorption



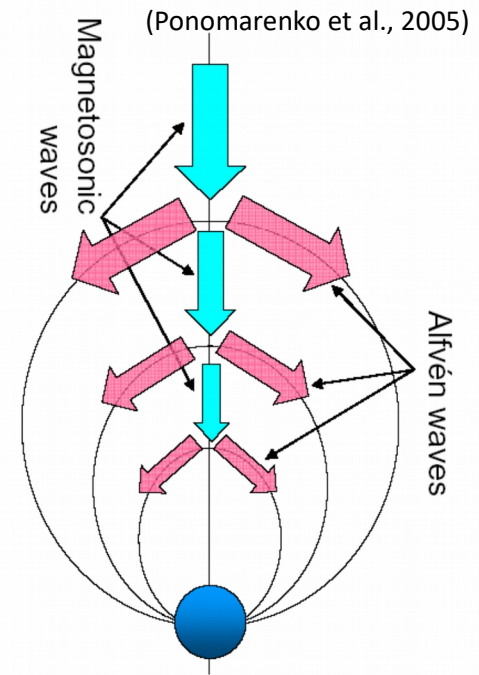
I
n
t
r
o
d
u
c
t
i
o
n



Meridional dependence of the toroidal and compressional fluctuations (CHAMP) (Heilig et al., JGR, 2013)

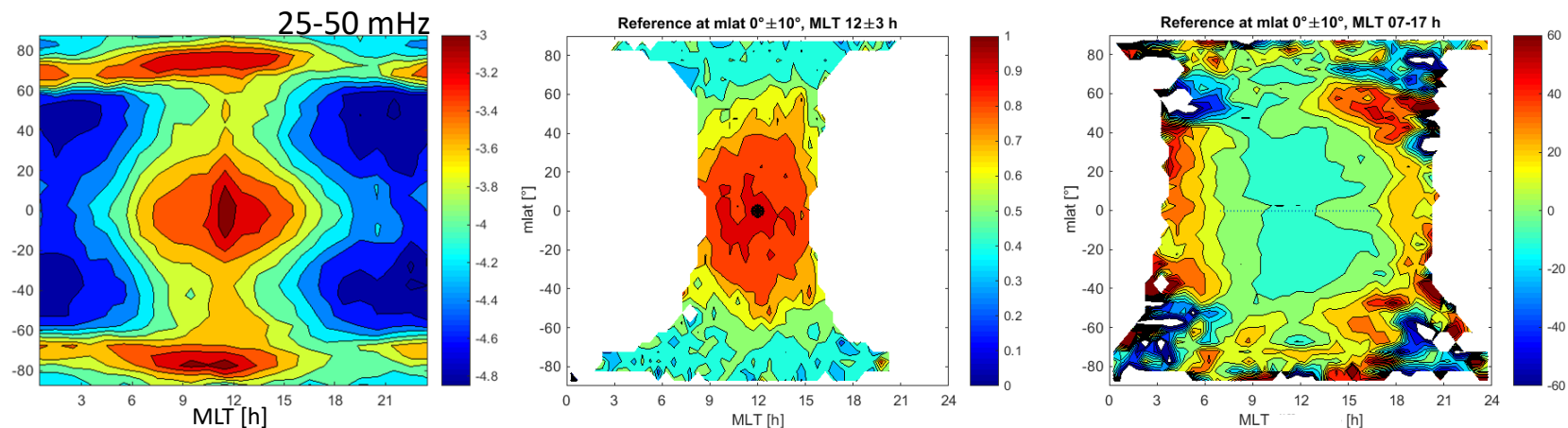
Two MHD modes in cold plasma:

- > compressional waves
- > Alfvén wave60s



CHAMP results confirm that mid latitude FLRs are driven by incoming compressional waves of upstream origin

Compressional Pc3 waves in the topside ionosphere



Swarm A normalized integral power
(Jan 2014- June 2016)

Swarm A-B coherence and phase difference (Jan 2014- June 2016)

(Heilig et al., JGR, 2016)

Compressional Pc3 waves are (2 spacecraft results)

Coherent on the dayside

In-phase on the dayside

every day phenomenon (dayside)

Large-scale compressional (> 10 000 km) waves with a wavefront ~ parallel to the ionosphere → compressional Pc3s of upstream origin can reach the ionosphere

Typical at frequency: 20-60 mHz, amplitude at CERN: few .1- few nT

Compressional Pc3 waves on the ground

Ground Pc3 activity (as driver of FLRs)

Dependence on SW/IMF parameters (Heilig et al., AnGeo 2010)

Clear dependence on solar wind density!

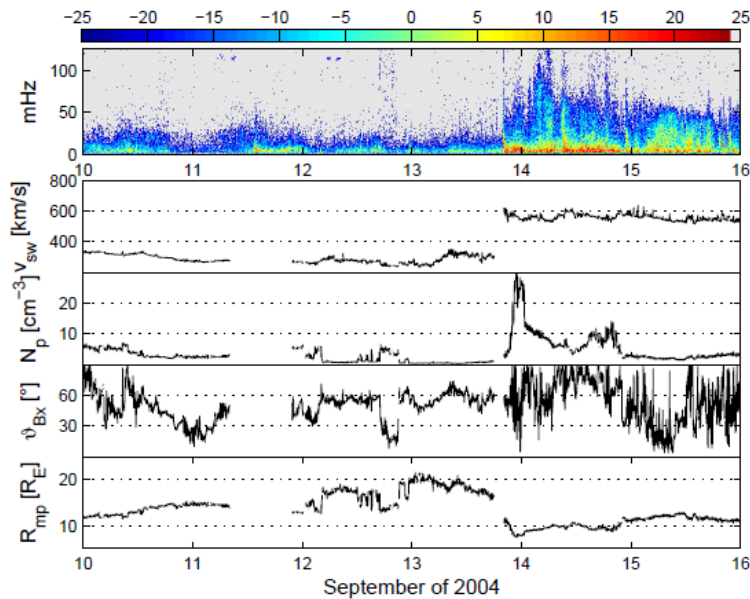


Fig. 2. SAE (13 September 00:00 UT–08:00 UT, 2004) embedded in a slow wind period prior to a fast solar wind stream arriving at 21:00 UT. Same format as Fig. 1.

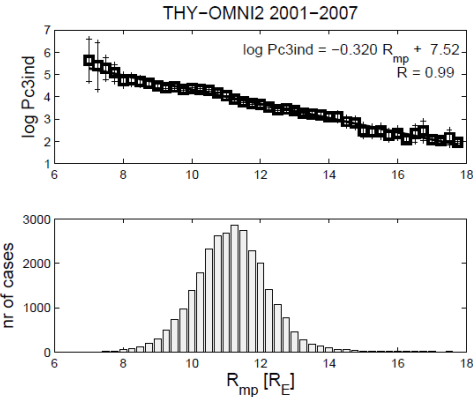


Fig. 4. THY log Pc3 index vs. standoff distance of the magnetopause (2001–2007). Same format as Fig. 3, but upper panel also includes the fitted curve, its equation, and the correlation coefficient of the fitted curve and the interval means.

... and on solar wind density dependent parameters, like the modelled MP standoff distance

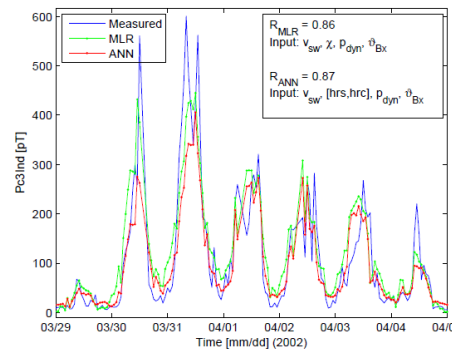
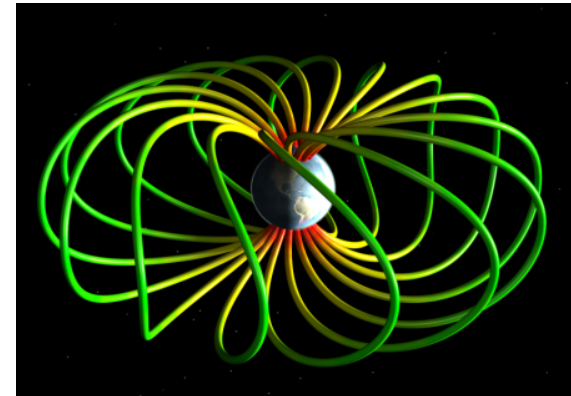
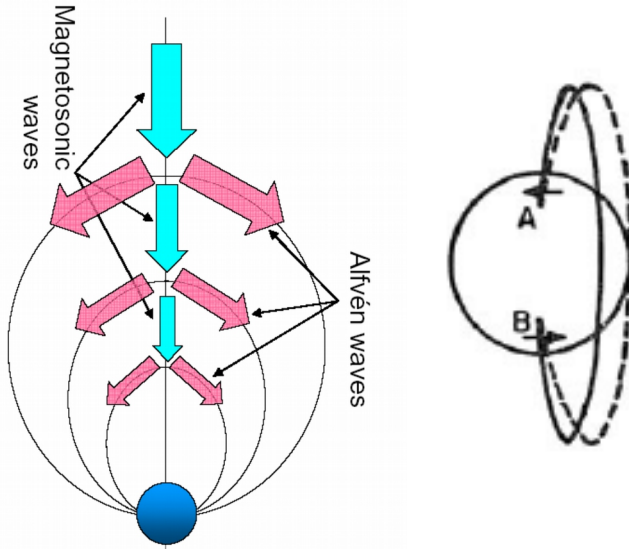


Fig. 13. Measured (solid curve) and modelled (red for ANN and green for MLR model) Pc3ind for a week included in the testing data set, using the optimal set of input parameters as indicated. The correlation between measured and modelled outputs are 0.87 for the ANN and 0.86 for the MLR model.

Comparison of derived multi-parameter Pc3 activity models (green: MLR, red: ANN) and the observed values (blue)

Field line resonances (Alfvén-mode)

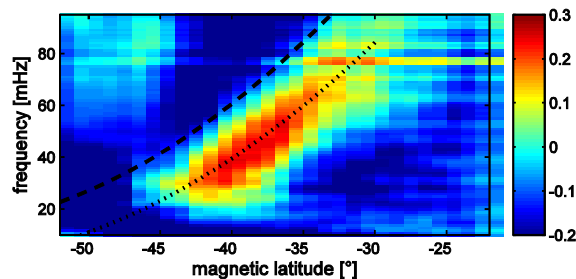
Effect of the ionosphere



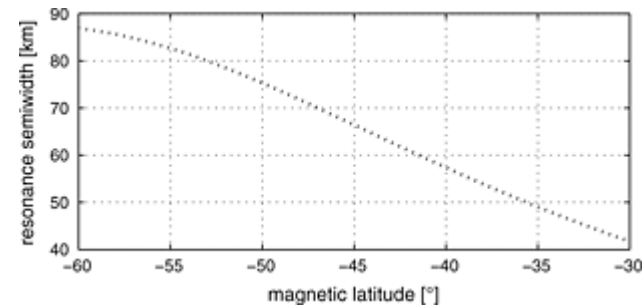
Field lines in a resonating shell

FLR is a standing Alfvén wave

Field line resonances are organized in **shells** (shell-resonance)



FLR freq. in space (dotted) is different from ground observations (dashed) due to Doppler-shift (due to s/c motion)

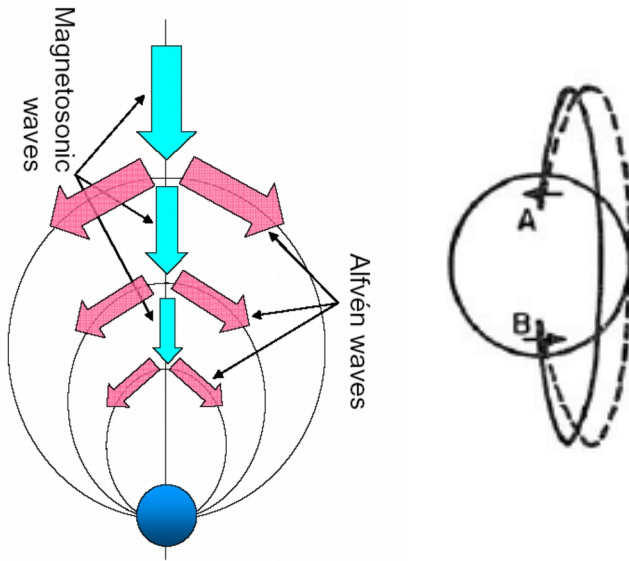


From the Doppler-shift the resonance width can be estimated (Heilig et al., 2013)

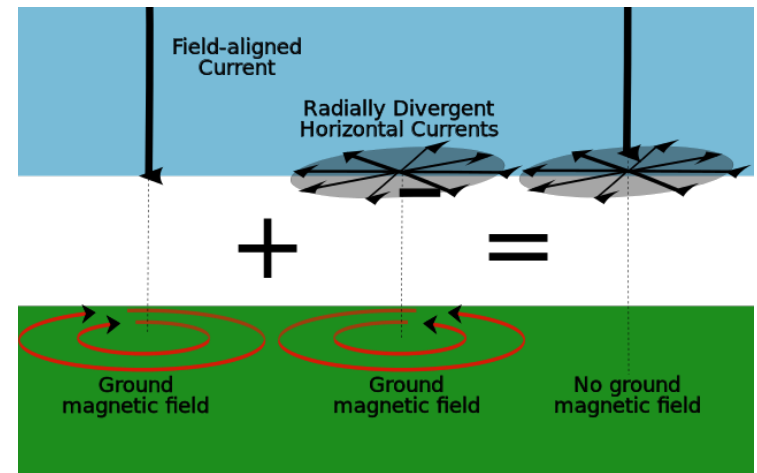
cross-shell scale: **resonance width few 10s kms**

Field line resonances (Alfvén-mode)

Effect of the ionosphere



Fukushima theorem



FLR is a standing Alfvén wave

1) with an associated field-aligned current (FAC) fluctuation

FACs feed divergent (Pedersen) currents in the ionosphere along E-field

Magnetic effect of FAC + divergent currents cancel each other = zero B-field

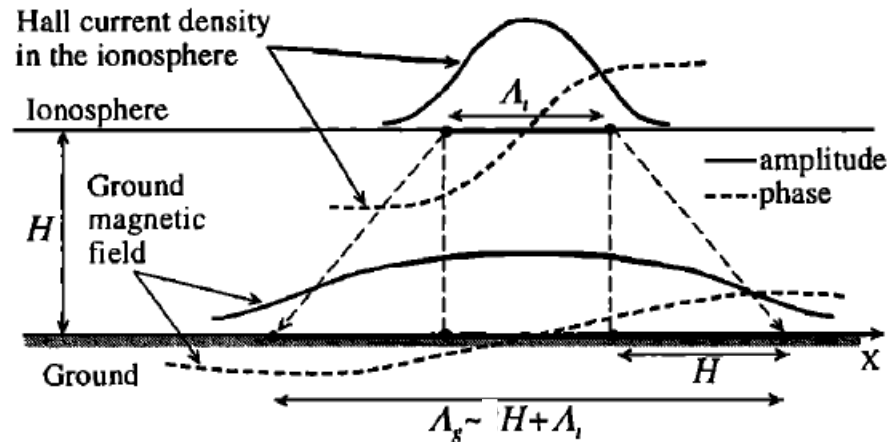
What is observed on the ground: dB from rotational Hall currents (perp. To both B- and E-field, not shown)

→ **90° rotation of the polarization ellipse** between space and ground: they appear in the north component (as compressional waves)

(North component is the most disturbed also for geomagnetic storms)

Spatial integration by the ionosphere

($h = 110$ km)



FLR: resonance width under the ionosphere

$$\delta_g = \delta_i + h$$

FLRs on the ground: 150-200 km meridional scale, 1000s kms in azimuthal scale

Typical frequency at CERN: $\sim 50 \pm 10$ mHz, amplitude: upto few nT

Transmission through the ionosphere ($h = 110$ km)

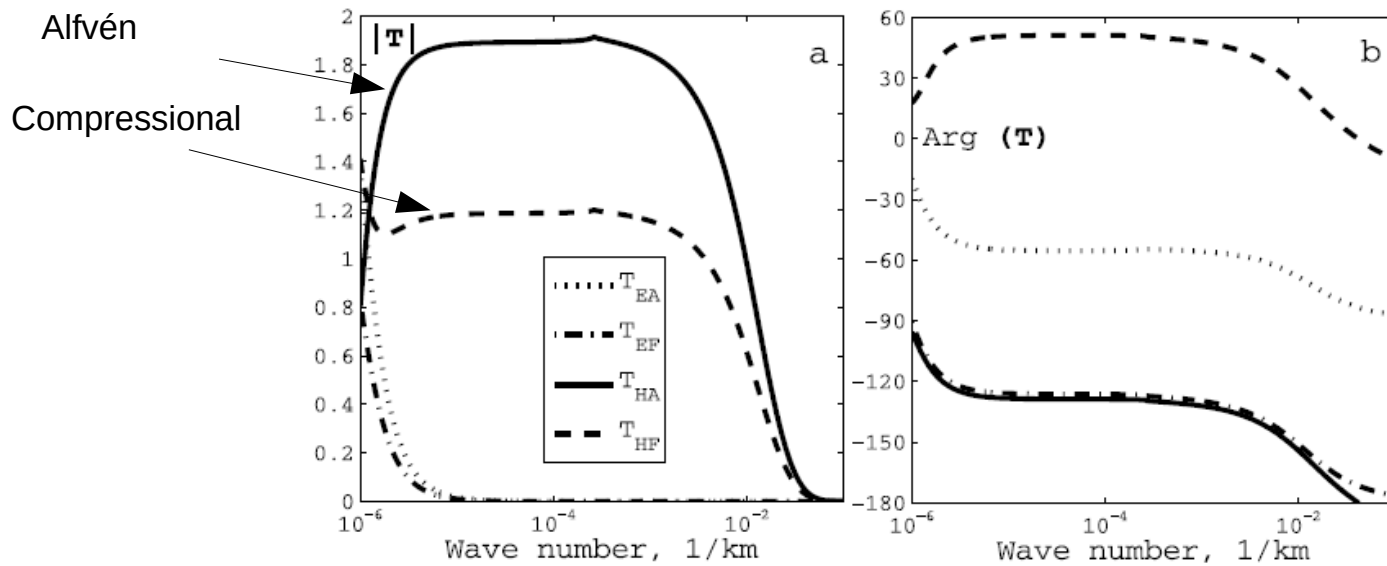


Figure 2. The dependence of different transmission coefficients T on the horizontal wave number for the daytime ionosphere (model 1), as in Figure 1.

Small scale waves (both compressional and Alfvén) heavily surpassed (model calculations)
 Small scale : below few hundred km (incident to the ionosphere)

(Pilipenko, Fedorov, Heilig, Engebretson, 2008)

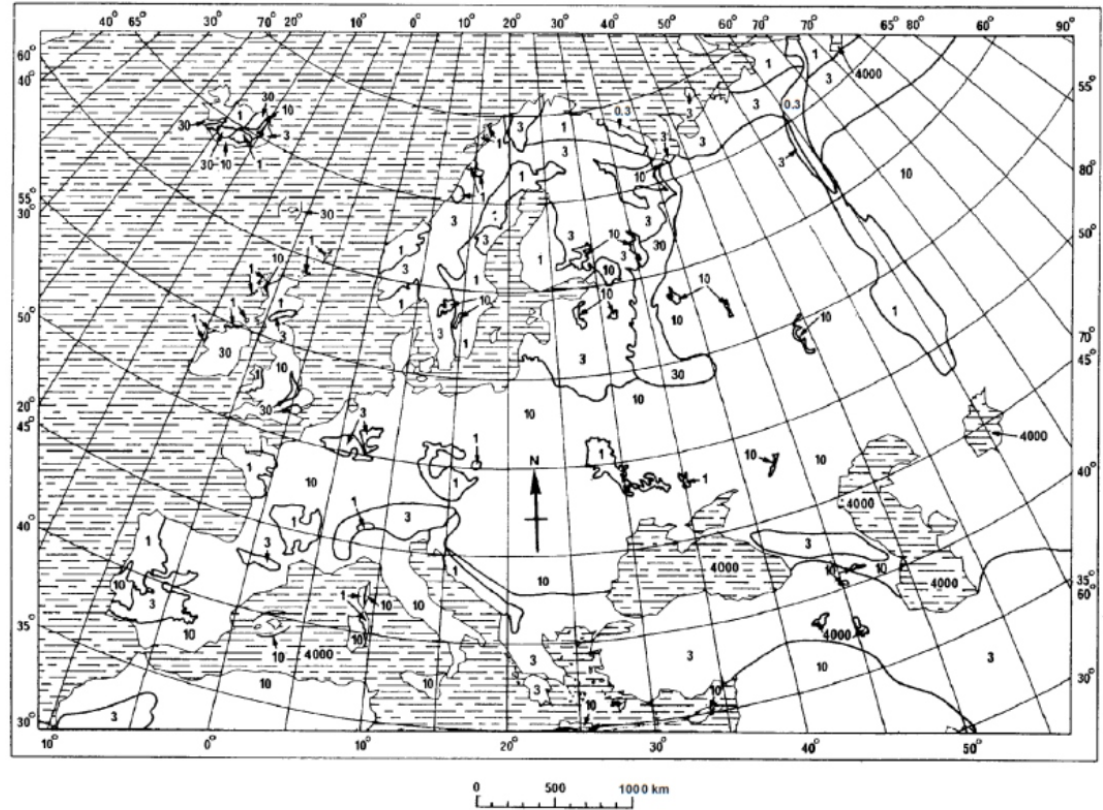
Penetration under the ground

Skin depth

$$\delta = \sqrt{\frac{2}{\mu_0 \sigma 2\pi f}} = 503 \sqrt{\frac{1}{\sigma f}} \quad (\text{m})$$

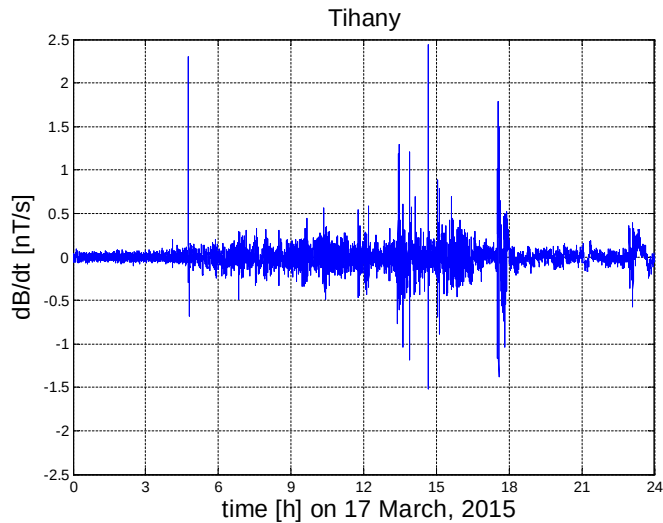
Ground conductivity σ is typically a few mS/m or a few tens of mS/m.

e.g. $\sigma = 4 \text{ mS/m}$, $f = 0.05 \text{ Hz} \rightarrow 35,6 \text{ km}$
 $\sigma = 40 \text{ mS/m}$, $f = 0.05 \text{ Hz} \rightarrow 11,2 \text{ km}$



ITU conductivity map for Europe
VLF range, in mS/m

Extremes at mid-latitudes



Rate of change in magnetic north component

Time scale: 1s

During storms it sometimes reaches a few nT/s

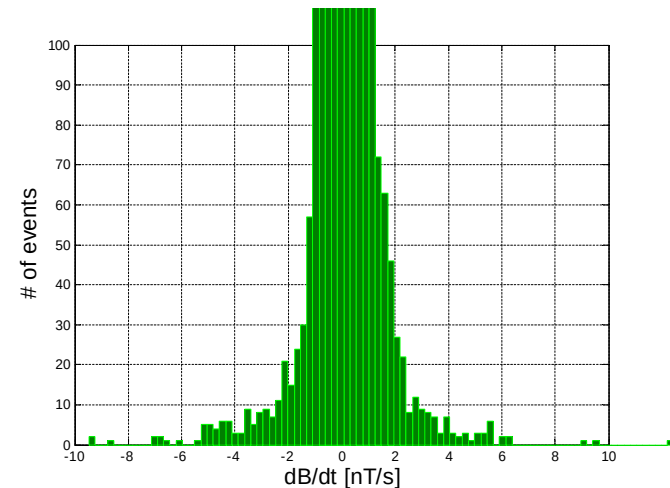
(,world record' is 770 nT/10 s Rorvik, Norway; 29 Oct, 2003)

How often?

Frequency of extremes

All measurement from 2015, Tihany

$|dB/dt| > 1$ # 707 \rightarrow twice a day
 $|dB/dt| > 2$ # 238 \rightarrow twice in three days



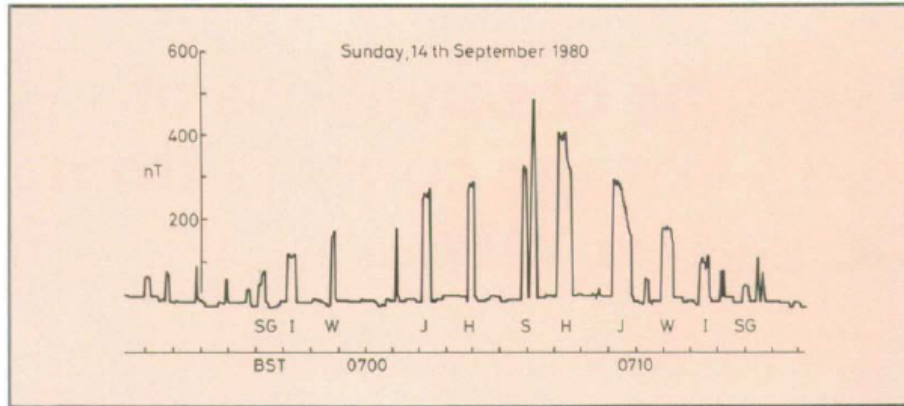
Summary for ULF wave part

- * ULF waves are everyday phenomena on ground
- * Fluctuation level depends on:
 - 1) solar wind conditions (different from geomagnetic storm drivers)
 - 2) local time (dayside more active)(nightside occasionally)
 - 3) latitudemay reach 10 nT at CERN latitude, typical: < 2 nT
- * Typical Pc3 frequency: 30-60 mHz at CERN latitude
- * Polarization of Pc3 waves (north-south daytime, near sunrise: east-west)
- * Spatial scales: meridional: 120-250 km (FLRs), >10000 km (compr.); azimuthal: >15000 km (compr.)
- * They propagate easily 100m underground with practically no attenuation

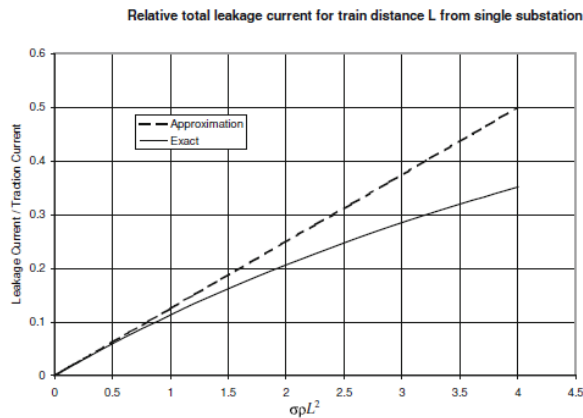
Incident ULF waves are probably not dangerous to CLIC (maybe extreme events)

Induced response in inhomogeneous conductivity (tunnel)???

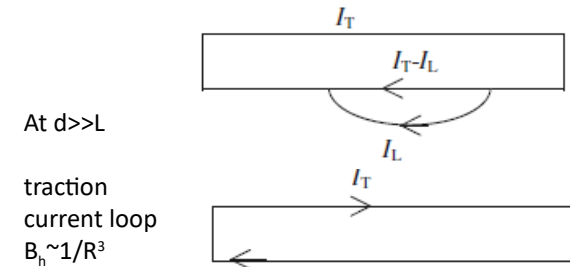
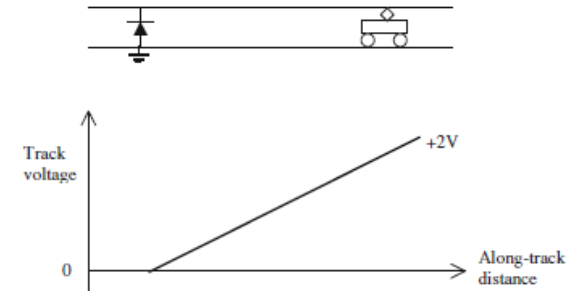
Stray fields from trains (DC case)



DC train noise as it travels from station 4 km along a track (there and back) recorded at 120 m from station H (Lowes, 1987)



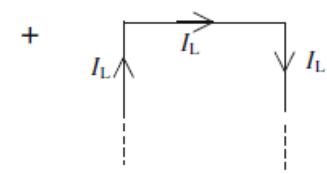
Leakage current can be 10s % of traction current (Lowes, 2009)



traction current loop
 $B_h \sim 1/R^3$

along track leakage current
 $B_z \sim 1/R^2$

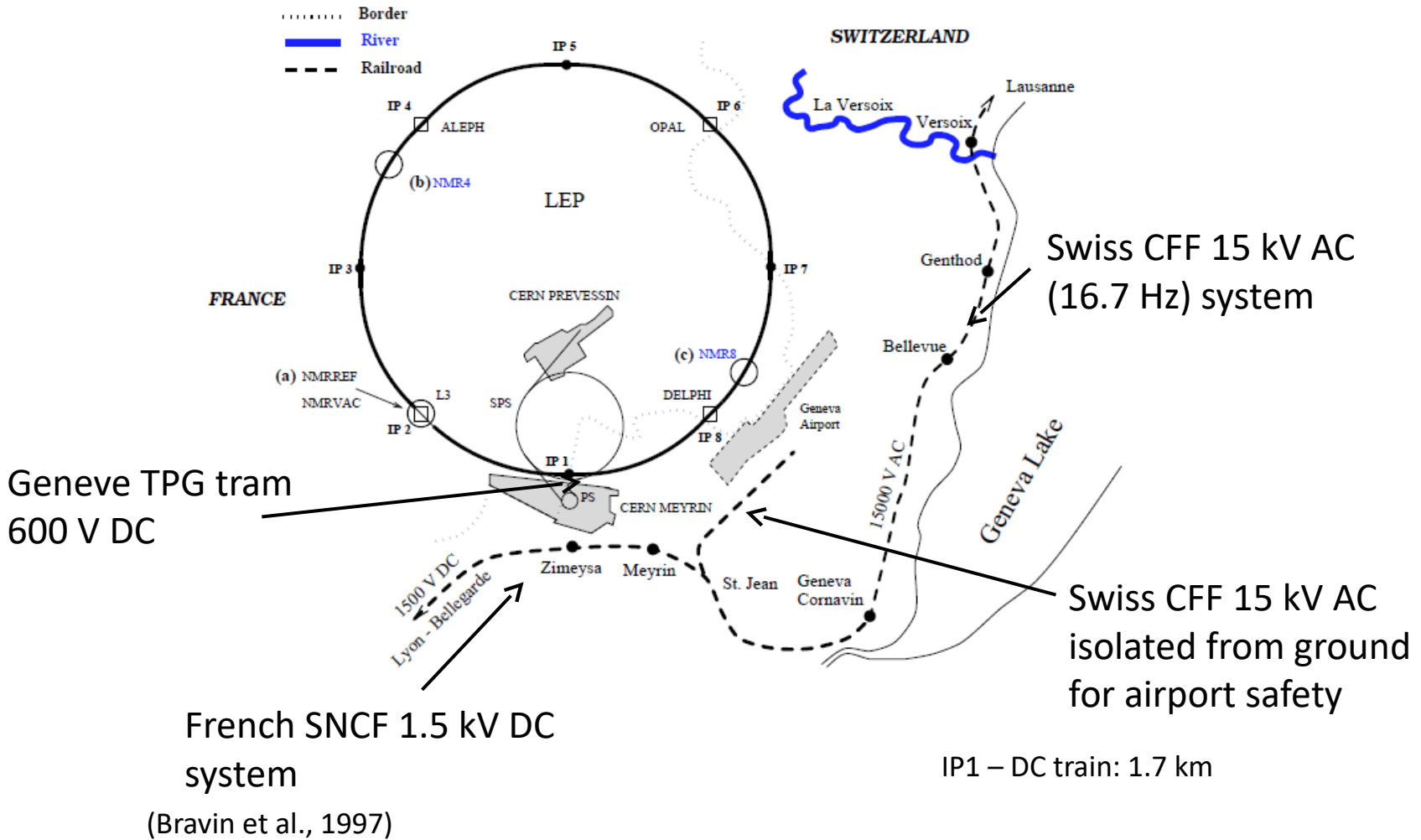
underground leakage current
 $B_h \sim 1/R$



100 A @ 1 km 10 nT

Simple model for DC trains (Lowes, 2009)

Stray fields from trains (DC case)



(Bravin et al., 1997)

Stray fields from trains (DC case)

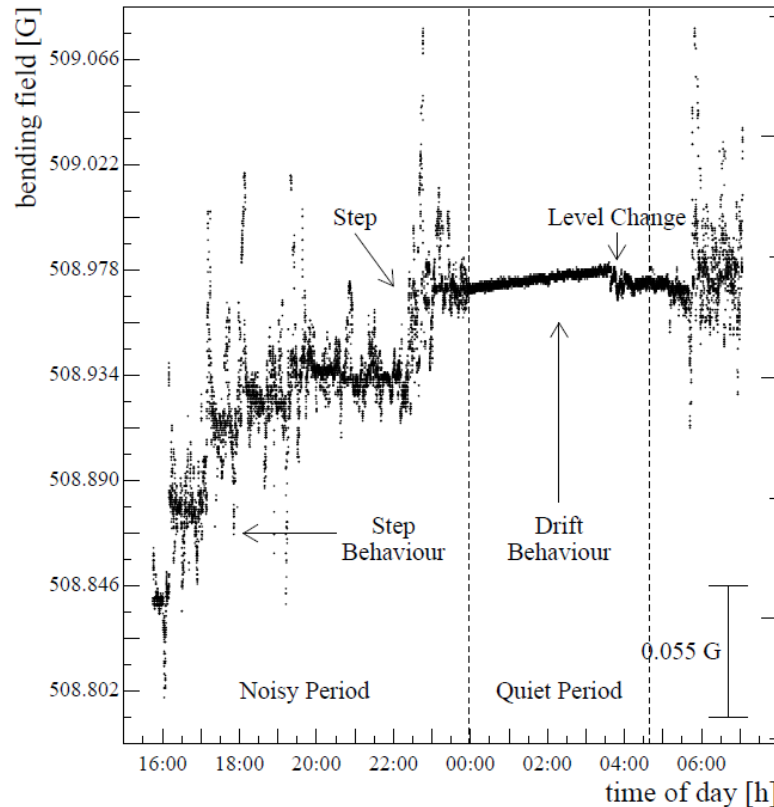
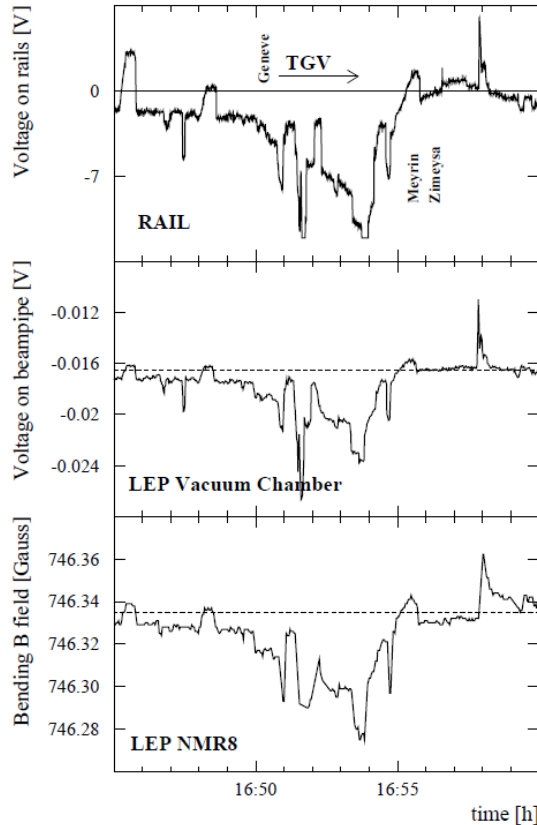


Figure 2: Magnetic field evolution measured in the tunnel by NMR8. The field increase during this period shows variations of the slope and steps of various sizes.

(Bravin et al., 1997)

Stray fields from trains (DC case)



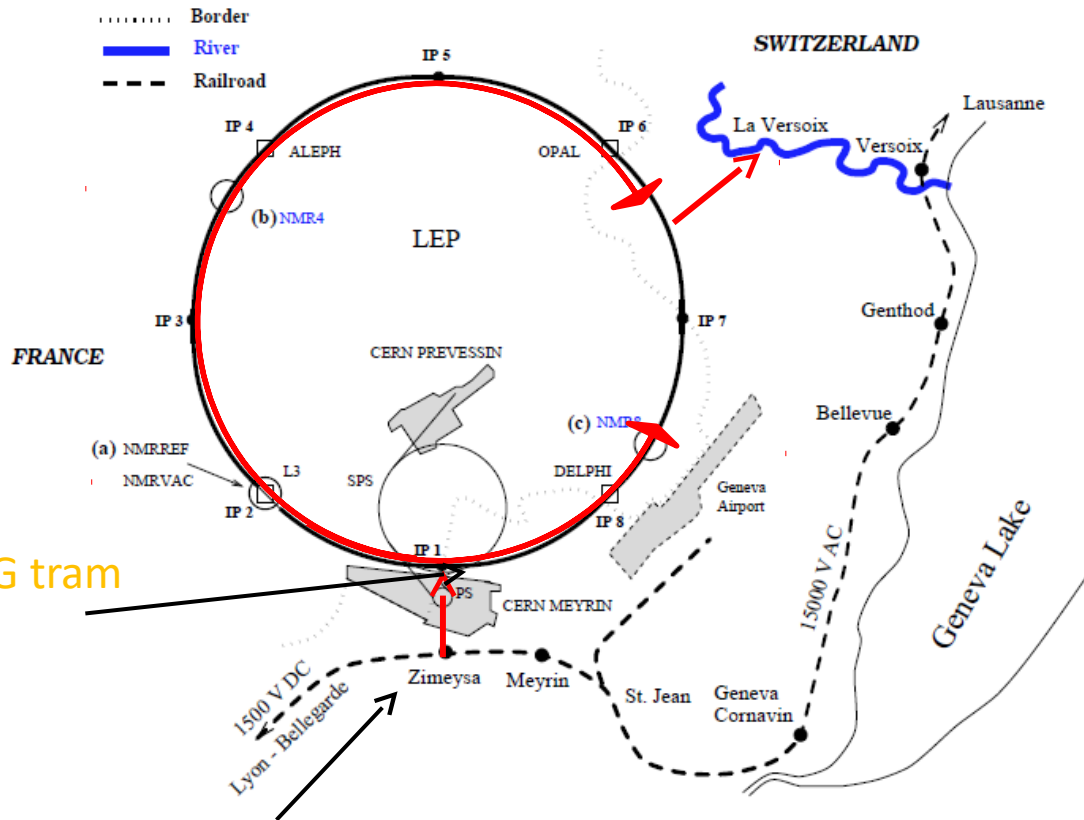
~ 1‰ of the voltage on rails leaked into the vacuum chamber

A few A current in vacuum chamber inside the bending magnet (Bravin et al., 1997)

magnetic field variation dB/B ~ 10^{-4}

Figure 3: Train leakage currents, vacuum chamber currents and the associated magnetic field perturbation on Nov. 13th, 1995. The observed peaks are coincident with the departure of the 16:50 Geneva-Paris TGV (SNCF).

Stray fields from trains (DC case)



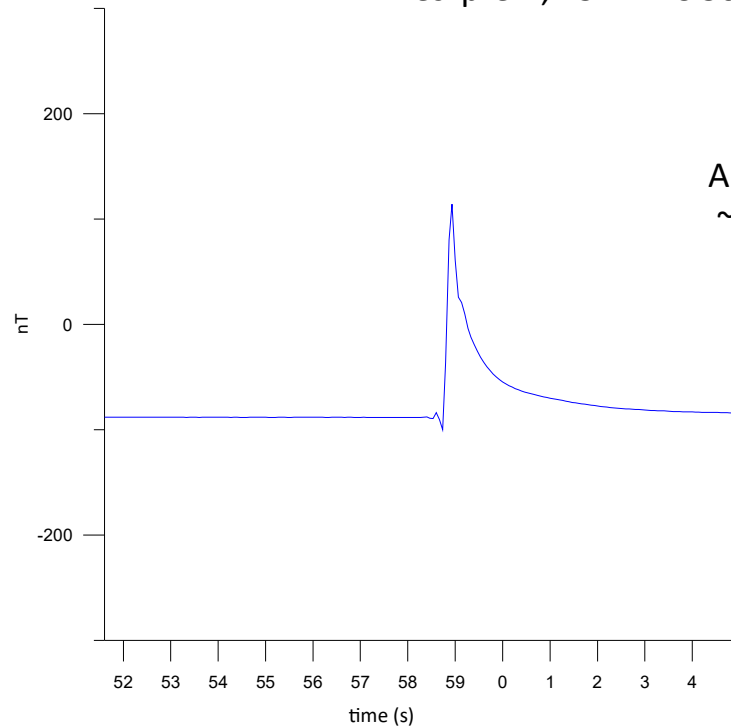
Geneve TPG tram
600 V DC

IP1 – DC train: 1.7 km

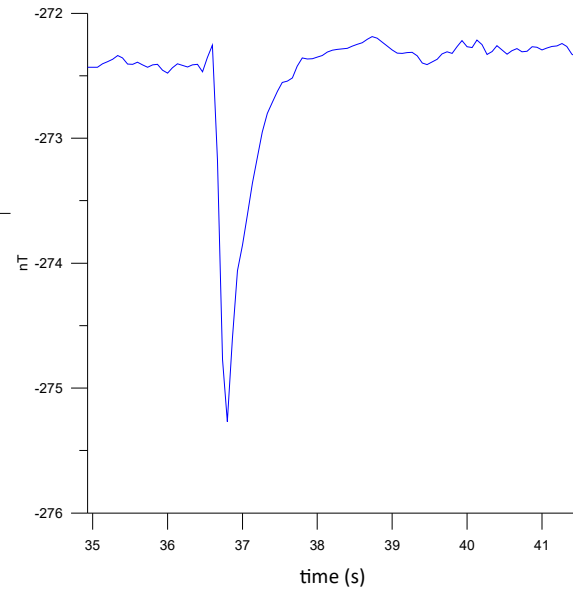
(Bravin et al., 1997)

Stray fields from trains (AC case)

Veszprém, 25 kV AC 50 Hz



A ~ 200 nT (vertical) impulse at ~ 50 m,
 ~ 3 nT (vertical) at ~ 1 km distance from a substation



Strange daytime signals at THY

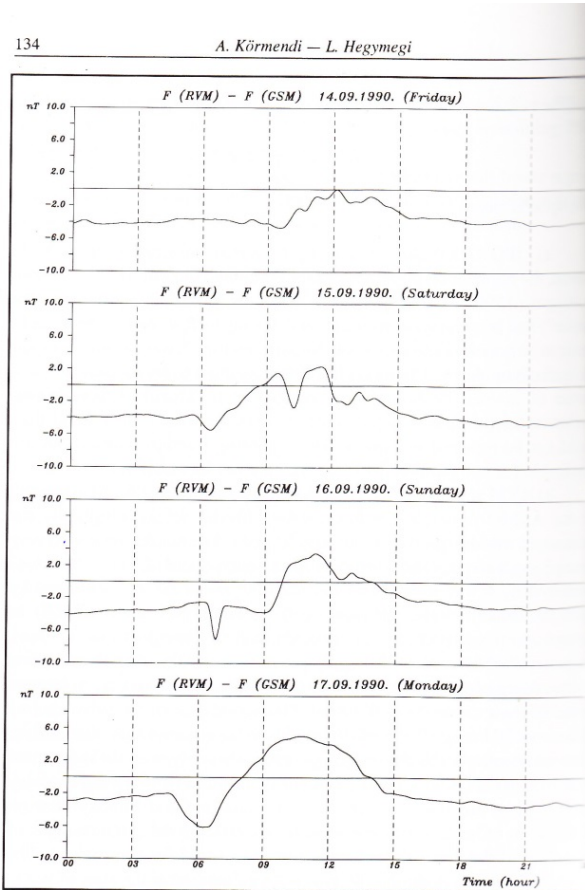


Fig. 4. Differences between the measured values by RVM and GSM
 4. ábra. RVM és GSM műszerek adatai közti különbség
 Рис. 4. Разница между показаниями приборов RVM и GSM

Daytime irregular signals in vertical component: exceeding 10 nT in total field. Source?

In a small hut with a dome shaped roof of copper painted 'silver'

appeared only at sunshine, not when clouds covered the Sun (temperature gradient)

Thermoelectric currents (Seebeck-effect, Cu roof painted with Al-based paint

$$S_{\text{Cu}} = 6.5 \mu\text{V/K}$$

$$S_{\text{Al}} = 3.5 \mu\text{V/K} \quad \Delta S = 3 \mu\text{V/K}$$

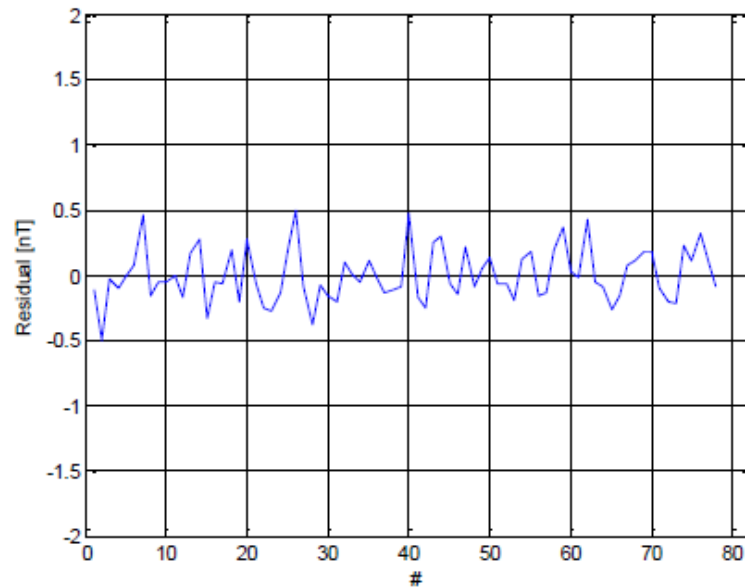
$$U_{\text{th}} = \Delta S * \Delta T = 3 \mu\text{V/K} * 40 \text{ K} = 120 \mu\text{V}$$

sheet current in this case

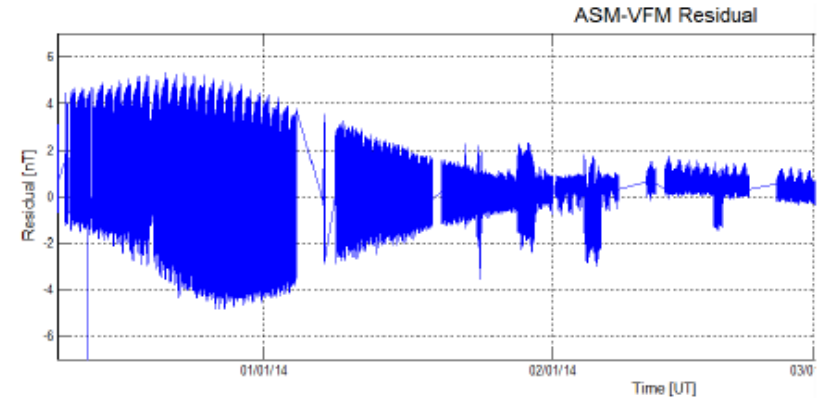
roof was cut into pieces and covered: effect gone

ASM/VFM residuals

- On-ground, the comparison of the VFM scalar values computed for all directions wrt. Absolute Scalar Magnetometer in constant background field of $50 \mu\text{T}$ gave: **$0.15 \text{ nT}_{\text{RMS}}$ ($\sim 1\text{ppm}$)**



- But In-flight, the same comparison gives few nT.

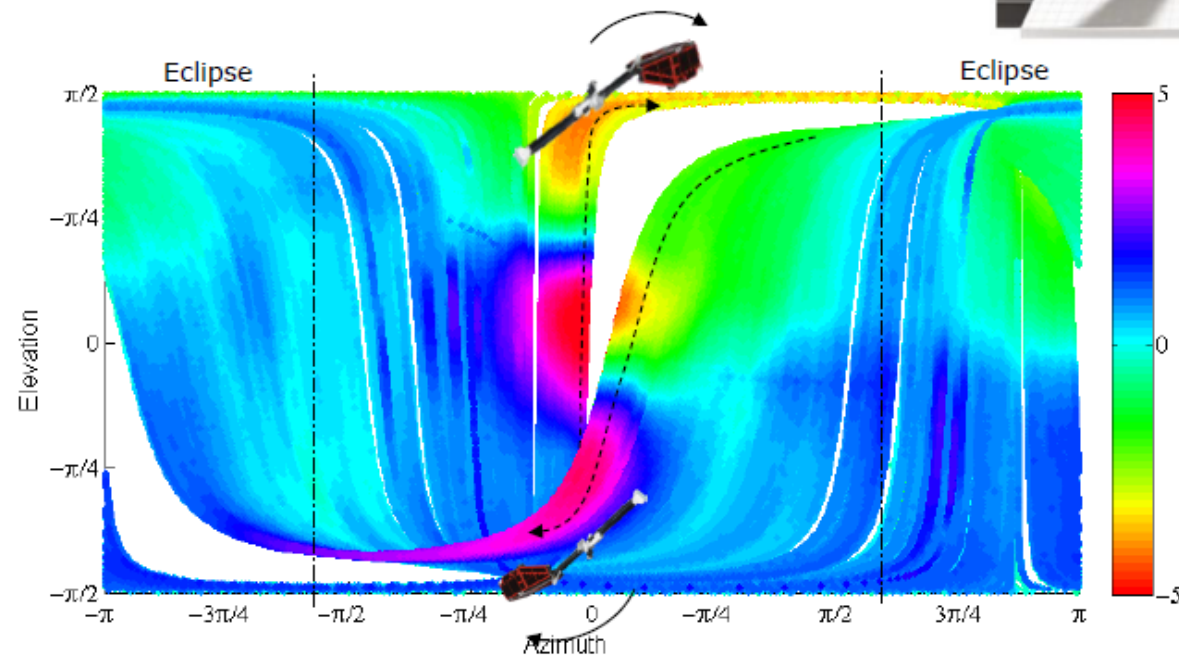
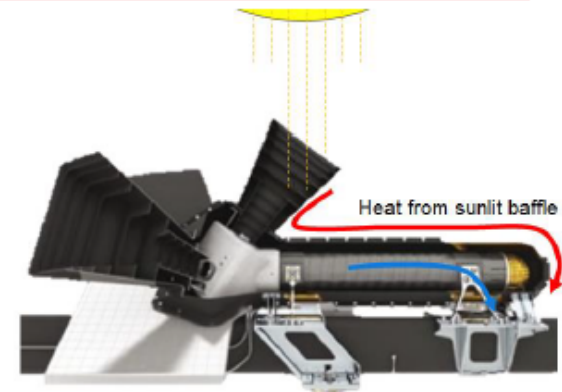


- On the night side, it is possible to reduce the residuals
- On the day side, they are modulated with LT, and maximum at $\text{LT}=12$

- Swarm A: $1.2 \text{ nT}_{\text{RMS}}$
- Swarm B: $0.9 \text{ nT}_{\text{RMS}}$
- Swarm C: $0.8 \text{ nT}_{\text{RMS}}$

ASM/VFM residuals (2)

- It appears that there is an external disturbance to the VFM, which causes the effect on the day side
- Thermo-electrical currents induced in the vicinity of the Optical Bench bracket under the VFM sensor

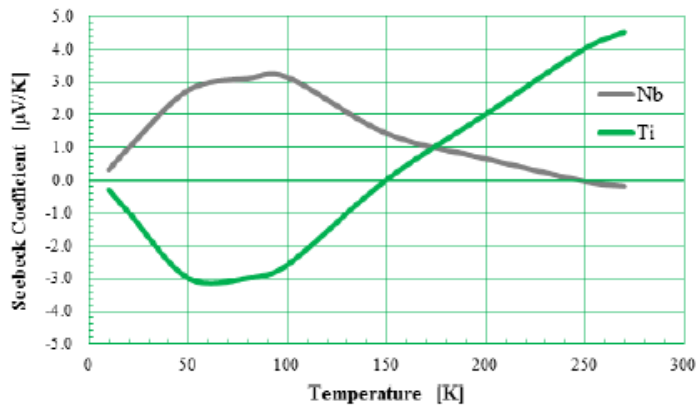


Thermocurrents in superconducting RF cavities

A Study of Thermocurrent Induced Magnetic Fields in ILC Cavities

Anthony C. Crawford Fermilab acc52@fnal.gov

The case of axisymmetric ILC type cavities with titanium helium vessels is investigated. A first order estimate for magnetic field within the SRF current layer is presented. The induced magnetic field is found to be not more than 1.4×10^{-8} Tesla = 0.14 milligauss for the case of axial symmetry. Magnetic fields due to symmetry breaking effects are discussed.



The Seebeck Coefficient for Niobium and Titanium at Low Temperatures

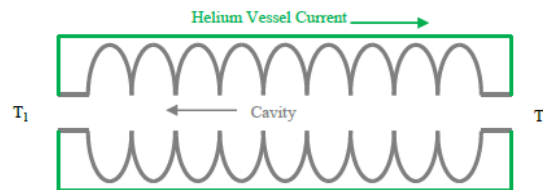


Figure 1. System Geometry

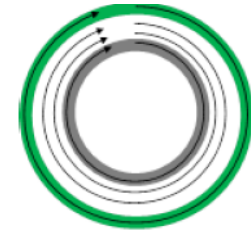


Figure 2. Magnetic Field Lines

Assumed: $\sim 170\text{K}$ temperature difference

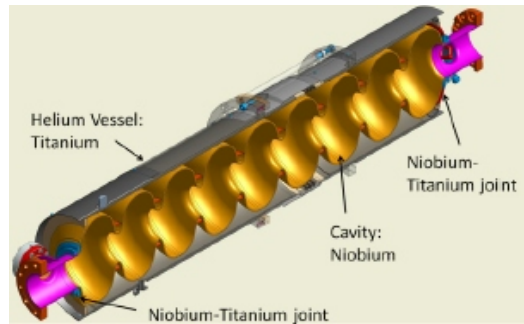
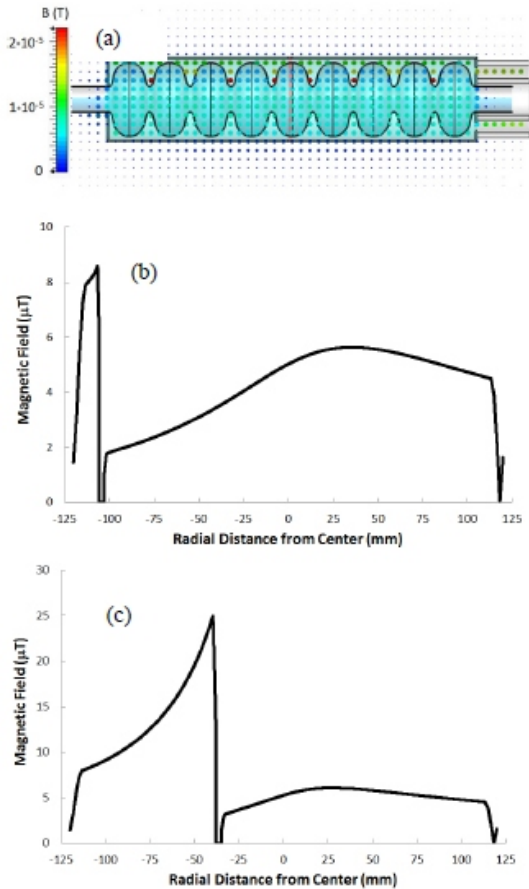
Estimated effect: 14 nT

Assuming axial symmetry

During cavity cooldown

(Crawford, A. C., 2014)

Thermocurrents in superconducting RF cavities



Eichhorn, R. and J. May-Mann (2015)
re-considered both the axial-symmetric and an
asymmetric (temperature gradient between top
and bottom) case
Resulting field: at microT level
Symmetric case: 4.8 A thermocurrent!

Figure 4: Results of the asymmetric calculation, where the lower portion of the cavity is assumed to be superconducting while the upper half remains normal conducting: 3-D field configuration (a), z-axis cuts along one equator (b) and at an iris (c).

Summary for stray currents

- * stray currents from environment (railway, CERN equipment) could be an issue: currents will follow the path where integral resistivity is minimum (e.g. beam pipe, waveguide, cables)
- * stray currents can be induced by natural, large-scale dB/dt (GIC, ULF, ELF, VLF) variations in the current loop formed by the tunnel and the surface (along rails?, through the lake?): magnetic flux variation inside the loop
- * stray currents maybe generated locally (e.g. longitudinal temperature gradients in a copper waveguide heated by RF power, in the beam pipe, if a loop is formed with some other material with different Seebeck-coefficient, e.g. in a sandwich shield: copper+mu-metal)